Food Chemistry: X 23 (2024) 101657

Contents lists available at ScienceDirect

Food Chemistry: X

journal homepage: www.sciencedirect.com/journal/food-chemistry-x

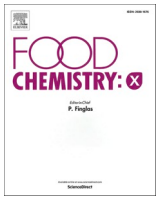

Ultrasound-assisted enzymatic extraction of soluble dietary Fiber from *Hericium erinaceus* and its in vitro lipid-lowering effect

Panling Yu [a,b], Xueyu Pan [b], Mingjie Chen [b], Jianshuai Ma [a,b], Baoting Xu [a,b], Yan Zhao [b,*]

[a] College of Food Science and Technology, Shanghai Ocean University, Shanghai 201306, China
[b] Institute of Edible Fungi, Shanghai Academy of Agricultural Sciences, Shanghai 201403, China

ARTICLE INFO

Keywords:
Hericium erinaceus soluble dietary fiber
Extraction process optimization
Monosaccharide composition
In vitro lipid lowering

ABSTRACT

Dietary fiber (DF) is an important active polysaccharide in *Hericium erinaceus*. Obesity can lead to a wide range of diseases. In this work, we investigated the in vitro lipid-lowering effect of soluble dietary fiber (SDF) from *H. erinaceus*, aiming to provide a basis for the subsequent development of lipid-lowering products. Ultrasound-assisted enzymatic extraction (UAEE) of SDF from *H. erinaceus* was performed. The optimal extraction parameters determined via single-factor experiments and response surface methodology (RSM) were as follows: Lywallzyme concentration, 1.0%; complex protease concentration, 1.2%; ultrasonication time, 35 min; and ultrasonication power, 150 W. In vitro lipid-lowering experiments revealed that the adsorption amount of cholesterol micelles by *H. erinaceus* SDF was 11.91 mg/g. The binding amount and binding rate of sodium taurocholate were 3.73 mg/g and 42.47%, respectively, and those of sodium glycocholate were 3.43 mg/g and 39.12%, respectively. The pancreatic lipase inhibition rate reached 52.11%, and the type of inhibition was competitive. Therefore, *H. erinaceus* SDF has good in vitro lipid-lowering ability.

1. Introduction

Hericium erinaceus is a fungus of the Odontococcaceae family and is commonly known as the monkey head mushroom; this mushroom is primarily distributed across China, North America, Japan, and Russia, among other regions. Fresh *H. erinaceus* are white or yellowish in color and become yellowish or yellowish brown after drying. The fruiting body is medium-sized, head-shaped or inverted egg-shaped, resembling the head of a monkey (Gerarda et al., 2023 Zhuang, Dong, Zhang, & Feng, 2023). As a rare species of edible and medicinal mushroom in China, *H. erinaceus* has broad application prospects and great market potential due to its unique appearance, flavor and health effects. Its fruiting bodies are rich in active ingredients, such as polysaccharides, proteins, sterols, fatty acids, erinacines, and hericenones (Liu et al., 2022; Liu et al., 2024; Yuan, Qiu, Yang, Liu, & Zhang, 2022). Among them, *H. erinaceus* polysaccharides are considered some of the main bioactive substances and have received widespread attention in nutritional health care applications (Liu et al., 2022; Tu, Liu, Wen, Chen, & Liu, 2021). Cai et al. (Cai et al., 2019) investigated the hypoglycemic effect of *H. erinaceus* polysaccharides on diabetic rats and reported that they significantly reduced fasting blood glucose levels, increased glucose tolerance and regulated glucose metabolism. Shang et al. (Shang et al., 2015) used broilers as experimental subjects and reported that *H. erinaceus* polysaccharides could reduce fat accumulation and promote cholesterol metabolism. Therefore, *H. erinaceus* has great value and prospects in the prevention and treatment of chronic diseases and their complications.

Dietary fiber (DF), which consists mainly of pectin, lignin, resins, pentaglycine, cellulose and hemicellulose, is defined as a multiple-unit carbohydrate polymer, a polysaccharide that is not digested by human intestinal enzymes (Minato, Laan, Die, & Mizuno, 2019; Sheng et al., 2019; Wang et al., 2021). DFs are naturally found in cereals, vegetables, fruits and nuts. DFs can be classified into two categories, soluble dietary fiber (SDF) and insoluble dietary fiber (IDF), on the basis of their solubility. SDF is easily digested by colonic microorganisms through the fermentative digestive system. SDF has good properties, with significant hypolipidemic, immunity-enhancing, hypoglycemic and antitumor activities (Bistriche, Hoffmann, & Wenzel, d. M. E., 2022; Farag, 2023; Perry & Wu, 2016; Guan, Yu, & Feng, 2021). Yang et al. (Yang et al., 2022) investigated SDF in oil tea seed residue and reported that it adsorbed cholesterol and inhibited pancreatic lipase activity, thus lowering blood lipid levels. Hua et al. (Hua et al., 2021) administered

* Corresponding author.
E-mail addresses: mjchen@saas.sh.cn (M. Chen), jiandan289@126.com (Y. Zhao).

https://doi.org/10.1016/j.fochx.2024.101657
Received 27 May 2024; Received in revised form 10 July 2024; Accepted 11 July 2024
Available online 14 July 2024

ginseng SDF to rats by gavage and found that ginseng SDF significantly improved the growth performance and serum antioxidant status of the rats and affected the level of immune oxidation. Ji et al. (Ji, Yu, Dong, & Liu, 2019) evaluated the in vitro antitumor activity of SDF from asparagus and reported that SDF effectively inhibited tumor growth and significantly improved the effects on splenic lymphocytes and NK cell activity. SDF plays an important role in the physiological functions of DF and is very beneficial to the human body. Therefore, it is crucial to develop effective techniques to improve the yield, quality and bioactivity of SDF. To date, research on polysaccharides from *H. erinaceus* and their utilization has focused mainly on soluble intracellular polysaccharides. Commonly used polysaccharide extraction methods include hot water methods, chemical methods, enzymatic methods, fermentation methods, etc. (Li et al., 2024; Li et al., 2024; Liu et al., 2024; Guo, Liang, Xiao, & Ge, 2023; Zhang et al., 2024). Conventional aqueous extraction of polysaccharides from *H. erinaceus* results in a considerable amount of residual material containing abundant cell wall polysaccharides, which are usually discarded without further extraction and utilization; this residue has great research and development value. Therefore, in this study, ultrasound-assisted enzymatic extraction (UAEE) was utilized to extract SDF from *H. erinaceus*. The results showed that ultrasonication caused violent shocks to the SDF particles, which led to the rupture of cell walls and membranes and the subsequent release of SDF molecules. Lywallzyme also destroys the cell structure, facilitating cell wall breakage and intracellular SDF extraction and greatly increasing the SDF yield. Wang et al. (Wang, Li, Lu, & Liu, 2024) used UAEE to extract polysaccharides from stone fungus, and the yield of polysaccharides was substantially increased by the use of UAEE. In their study, the polysaccharide yield was as high as 30.14%, and the antioxidant activity was enhanced. Chen et al. (Chen et al., 2023) used UAEE to extract polysaccharides from *Dendrobium officinale* and found that UAEE was able to efficiently extract polysaccharides in a shorter extraction time and at a lower extraction temperature than other extraction methods. The polysaccharides extracted by this method also had better functionality.

Along with rapid economic development, consumer dietary structure has changed due to overnutrition or imbalances, leading to obesity, cardiovascular disease, high blood cholesterol and type 2 diabetes mellitus; for example, the incidence of 'civilization disease' is increasing annually (Cassidy, McSorley, & Allsopp, 2018). Hyperlipidemia is the result of abnormal lipid metabolism in the body; specifically, it occurs when the concentration of serum lipids in the body exceeds the normal range. Hyperlipidemia is a high risk factor for cardiovascular diseases such as atherosclerosis, coronary heart disease and hypertension (Li, Chen, Wu, Su, Ding, Zhang et al., 2024; Sun et al., 2024). The treatment methods of diet-induced obesity complicated by hyperlipidemia mainly include lifestyle intervention and drug therapy. However, the drugs currently used for lipid-lowering therapy in clinical practice are mainly chemically synthesized, and long-term use of such drugs is likely to result in dependence, which can cause liver damage, muscle pain, gastrointestinal discomfort, and, in severe cases, even side effects such as rhabdomyolysis (Thanchanit & Pornanong, 2017). SDF is one of the essential nutrients for a balanced diet. Adequate supplementation of SDF is beneficial to intestinal health, as it regulates lipid metabolism to varying degrees, thereby reducing the risk of hyperlipidemia (Zhang et al., 2021; Qi et al., 2015; Zhang, Huang, & Ou, 2011). Therefore, dietary supplementation of SDF to reduce or prevent high blood lipid levels may be a good approach and has broad development prospects.

In this study, the extraction of SDF from *H. erinaceus* substrates via UAEE was optimized, and the effects of the Lywallzyme concentration, complex protease concentration, ultrasonication power and ultrasonication time on the yield of SDF were investigated. On the basis of the results, the basic components, molecular weight and monosaccharide composition of SDF were determined, and its in vitro lipid-lowering activity was investigated; the findings provide a theoretical basis for the development and utilization of SDF from *H. erinaceus*.

2. Materials and methods

2.1. Materials

Artificially cultivated *H. erinaceus* specimens were obtained from Guosen Biotechnology Co., Ltd., Institute of Edible Mushroom Research, Shanghai Academy of Agricultural Sciences (Shanghai, China). Images of the collected samples are shown in Fig. 1. Complex protease and α-amylase were purchased from Shanghai Solarbio Bioscience and Technology Co., Ltd. (Shanghai, China). Lywallzyme was purchased from the Guangdong Institute of Microbiology, China (Guangdong, China). Pepsin and trypsin were purchased from Shanghai Macklin Biochemical Technology Co., Ltd. (Shanghai, China). Pancreatic lipase was purchased from Shanghai Aladdin Biochemical Technology Co., Ltd. (Shanghai, China). Anhydrous ethanol was purchased from Shanghai Titan Technology Co., Ltd. (Shanghai, China). All reagents were of analytical quality. Distilled water was used throughout the experiments. Information on the apparatuses and equipment used in this experiment is given in Table S1 of the Supplementary Material.

2.2. Sample preparation

H. erinaceus samples were dried at 55 °C for 6–8 h, powdered, and then sieved through a 60 mesh sieve. The mushroom powder was stored in a desiccator at room temperature until further use.

2.3. Extraction of SDF from H. erinaceus

The UAEE method of Jia et al. (Jia et al., 2020) was used with some modifications. Mushroom powder (2 g) was mixed with 45 mL/g water, heated in a water bath at 100 °C for 4 h, and centrifuged at 4000 ×*g* for 20 min. The filtrate was adjusted to pH 5.8 and hydrolyzed with Lywallzyme at 27 °C for 1 h. The sample was heated again in a water bath at 100 °C for 4 h. The extracts were combined. The solution was concentrated under reduced pressure on a rotary evaporator to 1/5 the initial volume. The pH was adjusted to 7.0 with 0.1 mol/L HCl and 0.1 mol/L NaOH solutions. The samples were hydrolyzed with 1.5% α-amylase in an ultrasonicator at 55 °C for 2 h. The precipitate was removed by hydrolysis with 1.2% complex protease at 55 °C for 2 h, enzyme inactivation at 90 °C for 5 min, and centrifugation at 4000 ×*g* for 20 min. The supernatant was precipitated with 95% ethanol (4:1 *w/v*) for 12 h. The precipitate was collected by centrifugation (4000 ×*g*, 20 min), followed by washing with 70% ethanol, removal of the supernatant, and collection of the precipitate for drying at 50 °C to obtain SDF.

2.4. Single-factor experiments

The effects of the Lywallzyme concentration (%), complex protease concentration (%), ultrasonication time (min) and ultrasonication power (W) on the extraction rate of SDF from *H. erinaceus* were investigated using the extraction rate of SDF as an index. We selected the ranges of the four parameters by searching the relevant literature and performing preexperiments (Moczkowska, Karp, Niu, & Kurek, 2019; Shehzad, Minaxi, & Rajeev, 2021; Wen et al., 2020). The concentration of Lywallzyme was set to 0.2, 0.6, 1.0, 1.4, and 1.8%, the concentration of complex protease was set to 0.4, 0.8, 1.2, 1.6, and 2.0%, the ultrasonication time was set to 15, 25, 35, 45, and 55 min, and the ultrasonication power was set to 100, 125, 150, 175, and 200 W, respectively.

2.5. Response surface methodology (RSM) optimization of the extraction conditions

Compared with other methods, the combination of RSM and the Box–Behnken design (BBD) provides the best response values, saves time and money, and improves the efficiency and accuracy of experiments. The RSM-based experimental design using a three-level, four-factor

Fig. 1. Fresh samples of *H. erinaceus*.

combined BBD is shown in Table 1. Through single-factor experiments, low, medium and high factor levels were selected, and the extraction rate of *H. erinaceus* SDF was used as the response value.

2.6. Removal and purification of SDF

2.6.1. Protein removal via the Sevage method

First, 40 mL of chloroform was pipetted into a 100 mL stoppered conical flask; then, 10 mL of n-butanol was pipetted into the flask, and the mixture was mixed well and set aside in a place protected from light. A 5 mg/mL SDF solution was prepared; Sevage reagent (trichloromethane:n-butanol = 4:1) was added at a sample:Sevage reagent ratio of 4:1; the mixture was homogenized, shaken for 30 min, and centrifuged at 3000 ×*g* for 20 min; and the upper layer of the SDF solution was collected. The protein in the middle layer and the organic reagents in the lower layer were discarded. The deproteinization procedure was conducted in triplicate.

2.6.2. H_2O_2 Decolorization

H_2O_2 decolorization was performed according to the methods of Shao et al. (Shao, Sun, Liang, Li, & Li, 2020) with some modifications. A 10 mg/mL solution of *H. erinaceus* SDF was prepared and centrifuged at 6471 ×*g* for 30 min, and the supernatant was collected. The pH was adjusted to 8.0, and H_2O_2 solution (30% concentration) was added to reach a concentration of 3% relative to the total volume of the solution. Then, the pH was adjusted to 7.0 with 0.1 mol/L HCl and 0.1 mol/L NaOH solutions, the solution was placed in a water bath at 60 °C for 180 min, the mixture was centrifuged, and the supernatant was removed.

2.6.3. Removal of small molecules via Dialysis

After deproteinization by the Sevage method and decolorization by H_2O_2 treatment, the SDF solution was added to a 3500 Da dialysis bag, which was placed in deionized water and dialyzed for 48 h. The dialyzed solution was then precipitated by the addition of a fourfold volume of 95% alcohol and dried at 50 °C, after which the basic composition of the SDF was measured.

Table 1
Values of the test variables and the corresponding levels used in the process.

Independent Variables	Symbol	Levels		
		−1	0	1
Lywallzyme concentration (%)	X_1	0.2	1.0	1.8
Complex protease concentration (%)	X_2	0.4	1.2	2.0
Ultrasound time (min)	X_3	15	35	55
Ultrasound power (W)	X_4	100	150	200

2.7. Basic composition and structural characteristics of SDF

2.7.1. Basic composition

The direct drying method was used to determine the moisture content (Duan et al., 2022). A clean weighing flask was placed in a 100 °C drying oven, heated for 0.5–1.0 h, removed, covered, placed in a desiccator and cooled for 0.5 h. The flask was weighed, and the drying process was repeated. A total of 2.00–10.0 g of chopped or finely ground sample was added to this weighing flask. After the lid was set in place, the flask was precisely weighed, placed in a 100 °C drying oven to dry for 2–4 h, removed, placed in a desiccator to cool for 0.5 h and weighed again. Then, the samples were put in a 100 °C drying oven to dry for approximately 1 h, removed, put in a desiccator to cool for 0.5 h and then weighed. The differences in mass before and after the second round of drying were not >2 mg; that is, the mass was constant. The difference between the weight of the sample before and after drying was considered the moisture content of the sample.

The protein content was determined using the Thomas Brilliant Blue method according to the instructions of the Bradford Protein Concentration Assay Kit (Solarbio Products). A total of 0.5 mL of protein standard preparation solution was added to 80 mg of protein standard, which was fully dissolved to form a protein standard solution (160 mg/mL). A 160 mg/mL SDF solution was prepared as a control. Three test tubes were used: a blank tube, a standard tube and an assay tube. First, 0.04 mL of distilled water and 2 mL of bisulfite reagent were added to the blank tube. To the standard tube, 0.04 mL of protein standard solution and 2 mL of bisulfite reagent were added. To the assay tube, 0.04 mL of SDF sample and 2 mL of bisulfite reagent were added. The solutions were mixed separately and incubated at 37 °C for 10 min. No additional solutions were added to the blank tube, and the absorbance of the solution in each tube was measured at 540 nm. The protein content in the sample (g/L) was calculated as the absorbance of the assay tube divided by the absorbance of the standard tube multiplied by the concentration of protein standard solution (g/L).

The starch content was determined by using a Starch Content Assay Kit (Boxbio Products) with reference to the literature (TANAKA, OKAMOTO, MATSUSHIMA, OTA, MATSUMOTO, & AKASAKI Tanaka et al., 2013). Fifty milligrams of SDF was weighed in a centrifuge tube, and 1 mL of eluent was added. The mixture was mixed thoroughly, incubated in an 80 °C water bath for 30 min, and centrifuged at 3000 ×*g* for 5 min at room temperature. The supernatant was discarded, and the precipitate was collected. Then, 500 μL of distilled water was added to the precipitate, which was mixed thoroughly and incubated at 95 °C for 15 min. After cooling to room temperature, 1 mL of extraction solution was added, and the mixture was extracted for 15 min at room temperature. The mixture was subsequently centrifuged at 3000 ×*g* for 10 min at room temperature, after which the supernatant was collected. Three 2

mL centrifuge tubes were used as the measurement tube, standard tube and blank tube. Two hundred microliters of the sample to be tested and 1000 μL of color development solution were added to the assay tube. To the standard tube, 200 μL of standard dilution solution and 1000 μL of color development solution were added. A 10 mg/mL glucose standard solution was diluted with distilled water to 0.12, 0.10, 0.08, 0.04, 0.02, and 0.01 mg/mL. Two hundred microliters of distilled water and 1000 μL of color development solution were added to the blank tube. Each tube was placed in a 95 °C water bath for 10 min and then cooled to room temperature. The absorbance of each sample was measured at 620 nm. The absorbances of both the assay tube and the standard tube were corrected by the absorbance of the blank tube. A linear regression equation was obtained by plotting 0.12, 0.10, 0.08, 0.04, 0.02, and 0.01 mg/mL on the horizontal axis and the corresponding absorbances of the standard tube on the vertical axis; the absorbance of the assay tube was substituted into the equation to obtain the starch content in the sample (mg/mL).

The ash content was determined by an ashing and drying method according to previous methods (J., D., A., & T., 2023). After the sample (5 g) was weighed, it was heated to a low temperature to ensure complete charring without smoke, after which it was placed in a muffle furnace and combusted at 550 ± 25 °C for 4 h. was After the furnace cooled to approximately 200 °C, the sample was removed, put into a desiccator and cooled for 30 min. Combustion was repeated until the sample reached a constant weight, and then the ash content was calculated (given as the weight percentage in g/100 g, abbreviated as %).

The SDF content was determined via the enzyme weight method (Lily, Afaf, Usama, Leila, & Serene, 2023). Approximately 1 g of the SDF sample was accurately weighed, and 40 mL of 0.05 mol/L MES-Tris buffer was added. Then, 50 μL of 0.8% α-amylase solution was added to the sample solution, which was slowly stirred, covered with aluminum foil, and placed in a 95 °C constant temperature oscillating water bath for 35 min. The beaker was removed, and the mixture was cooled to 60 °C. The sample solution was placed in a water bath at 60 °C, 100 μL of 1.0% protease solution was added to each beaker, and the mixture was allowed to react for 30 min. The aluminum foil lid was opened, 5 mL of 3 mol/L acetic acid solution was added while stirring, and the temperature was controlled at 60 °C. The pH of the sample solution was adjusted to 1.5 with 0.1 mol/L sodium hydroxide solution and 0.1 mol/L hydrochloric acid solution. Then, 100 μL of starch glucose velvetting enzyme solution was added under stirring, and the reaction was continued in a water bath at 60 °C for 30 min. All the enzyme solutions were transferred to a crucible for filtration, and the residue was washed with hot water (70 °C, 10 mL) 2 times. The filtrates were collected and combined, and the mixture was centrifuged at 3000 ×*g* for 10 min. The supernatant was collected and centrifuged at 3000 ×*g* for 10 min, and the volume of the filtrate was increased by adding 1-fold 95% ethanol preheated to 60 °C. The mixture was precipitated at room temperature for 1 h. After centrifugation at 3000 ×*g* for 10 min, the precipitate was collected and dried at 50 °C, after which the sample was weighed to obtain the SDF content.

2.7.2. Structural characteristics

2.7.2.1. Molecular mass distribution. The relative molecular mass distribution of SDF was analyzed using a Waters 2695 high-performance liquid chromatography (HPLC) system with TSK PWXL6000 and TSK PWXL4000 tandem columns and a 2414 differential refractive detector. The relative molecular mass distribution of SDF was analyzed with a DAWN8+ laser detector. In accordance with the literature (Liu et al., 2013), the mobile phases used were 0.15 mol/L $NaNO_3$ and 0.05 mol/L $NaH_2PO_4{\cdot}2H_2O$ (pH 7.0, containing 0.02% sodium azide by mass); the flow rate was 0.5 mL/min; and the chromatographic column temperature was held constant at 35 °C. The refractive index detector temperature was 35 °C. The wavelength of the laser detector light source was 623.8 nm, and the refractive index increment (dn/dc) of SDF in solution was calculated on the basis of 0.146 mL/g. A 3 mg/mL SDF solution was prepared using the mobile phase. After centrifugation at 12000 ×*g* for 20 min, the supernatant was collected and analyzed by high-performance size exclusion chromatography multiangle laser light scattering refractive index (HPSEC-MALLS-RI) analysis. Finally, the light scattering data were collected and analyzed using Astra (version 6.1.1; Wyatt Technology, Santa Barbara, CA) data analysis software to calculate the relative molecular mass.

2.7.2.2. Determination of monosaccharide composition. The method of Yuan et al. (Yuan et al., 2022) was followed and appropriately modified. The monosaccharide composition of SDF was determined by high-performance anion-exchange chromatography (HPAC). Two milligrams of the SDF sample was hydrolyzed by adding 3 mL of 2 mol/L trifluoroacetic acid (TFA) to the sample and placing the mixture in an oil bath at 110 °C for 4 h. The hydrolyzed product was repeatedly blown dry by nitrogen blowing with several additions of methanol until it had no acidic odor. The hydrolysate was dissolved in ultrapure water, centrifuged, and diluted, and its monosaccharide composition was determined via ion chromatography.

The following standards were used: galactose, glucose, arabinose, fucose, rhamnose, mannose, xylose, glucuronic acid and galacturonic acid. Chromatographic conditions: column, CarboPac PA-20 anion-exchange column (150 mm × 3 mm i.d.); injection volume, 25 μL; volume flow rate, 0.45 mL/min. The column temperature was 30 °C, and the mobile phases were ultrapure water and 0.25 mol/L sodium hydroxide (NaOH).

2.8. In vitro study of the lipid-lowering mechanism of SDF

2.8.1. Oil adsorption

The oil adsorption method of Yan et al. was used with modifications (Yan, Hu, Yang, & Zhao, 2018). SDF (2.00 g, W_1) was placed in a 50 mL centrifuge tube, to which 16 *g* of edible soybean oil was added, and the tube was incubated in a constant-temperature shaker at 37 °C for 1 h. Subsequently, centrifugation was carried out at 4000 ×*g* for 20 min, the upper layer of oil was discarded, and the residue was blotted dry with filter paper and weighed to obtain W_2. The amount of SDF-bound oil and fat is expressed in g/g and was calculated with Eq. (1).

$$\text{Oil absorption} = \frac{(W_2 - W_1)}{W_1} \quad (1)$$

2.8.2. Cholesterol micelle adsorption

Cholesterol micellar solution (1 mL) containing 10 mmol/L sodium taurocholate, 10 mmol/L sodium glycocholate, 5 mmol/L cholesterol, 5 mmol/L oleic acid, 132 mmol/L sodium chloride (NaCl), and 15 mmol/L PBS (pH 7.4) was prepared by homogenization using ultrasonication according to the literature (Raederstorff, Schlachter, Elste, & Weber, 2003). Aliquots (3 mL) of micellar solution were pipetted into six 100 mL conical flasks to which 70, 90, 110, 130, 150, or 170 mg of SDF was added. The flasks were incubated for 2 h at a constant temperature of 37 °C with shaking and then centrifuged at 4000 ×*g* for 20 min. The supernatants were collected, and the cholesterol content in the supernatants was determined via the appropriate kit; no SDF was added to the blank. The total cholesterol (TC) content assay kit was obtained from Sangon Biotech (Shanghai) Co., Ltd. The cholesterol content bound to SDF was calculated as the cholesterol content in the blank solution minus the cholesterol content in the sample mixture.

2.8.3. Bile salt adsorption

2.8.3.1. Determination of bile salts and preparation of standard curves. The method of Wang et al. (Wang, Yu, Zang, & Ye, 2018) was referenced

and appropriately modified. Predetermined volumes of sodium taurocholate (0.3 mmol/L) and sodium glycocholate (0.1 mol/L in pH = 6.3 phosphate buffer solution (PBS)) (0, 0.1, 0.5, 1.0, 1.5, 2.0, or 2.5 mL) were pipetted into 10 mL stoppered test tubes, to which 0.1 mol/L PBS (pH = 6.3) was added to bring the volume to 2.5 mL; 7.5 mL of 60% sulfuric acid solution was added, and the solution was cooled to room temperature after reaction in a water bath at 70 °C for 20 min. The reaction solutions were subjected to a full-wavelength scan to determine the maximum absorption wavelength, and the standard curves of the two bile acid salts were plotted.

2.8.3.2. Binding of bile salts in vitro. In accordance with the literature (Zhou, Xia, Zhang, & Yu, 2005), 10 mg/mL solutions of pepsin and trypsin were prepared in 0.1 mol/L PBS (pH 6.3) and set aside. SDF (150 mg) was added to a 20 mL test tube and successively combined with 1 mL of 0.01 mol/L HCl solution and 3 mL of pepsin; the mixture was digested with constant-temperature oscillation at 37 °C for 1 h to simulate the gastric environment. Then, 4 mL of trypsin was added, the pH was adjusted to 6.3 with 0.1 mol/L NaOH solution, and digestion was carried out with constant-temperature oscillation at 37 °C for 1 h to simulate the intestinal environment. Afterward, 4 mL of bile acid salt solution (0.3 mmol/L sodium taurocholate solution and 0.3 mmol/L sodium glycocholate solution, both prepared with 0.1 mol/L PBS buffer at pH 6.3) was added to each sample, and the samples were shaken for 90 min at a constant temperature of 37 °C, transferred to 50 mL centrifuge tubes, and then centrifuged for 20 min at 4000 ×*g*. The supernatant was collected, and the bile acid salt content was determined.

2.8.3.3. Colorimetric determination of bile salts. A total of 2.5 mL of the supernatant collected in Section 2.8.3.2 was placed in a 10 mL test tube, 7.5 mL of 60% sulfuric acid was added, and the tube was placed in a water bath at 70 °C for 20 min. Then, the sample was removed and cooled to room temperature, and the absorbance value was determined at the maximum absorption wavelength. The concentration of each bile salt in the sample solution was determined by using a standard curve. The binding rate of SDF to each bile salt was determined via Eq. (2) and Eq. (3).

$$\text{Binding rate of sodium glycocholate}(\%) = \frac{\text{Addition of sodium glycocholate} - \text{Surplus of sodium glycocholate}}{\text{Addition of sodium glycocholate}} \times 100 \quad (2)$$

$$\text{Binding rate of sodium taurocholate}(\%) = \frac{\text{Addition of sodium taurocholate} - \text{Surplus of sodium taurocholate}}{\text{Addition of sodium taurocholate}} \times 100 \quad (3)$$

2.8.3.4. Adsorption kinetics of bile salts by SDF. The procedure described in Section 2.8.3.2 was followed through the addition of bile acid salt solution; the resulting mixture was shaken at 37 °C for 20 min, 30 min, 60 min, 90 min, or 120 min, transferred to a 50 mL centrifuge tube and centrifuged at 4000 ×*g* for 20 min, after which the content of bile salts in the supernatant was determined according to the method in Section 2.8.3.3.

2.8.3.5. Effect of SDF addition on bile salt adsorption. First, 70 mg, 110 mg, 150 mg, 190 mg or 230 mg of SDF was weighed into a 100 mL stoppered triangular flask, and the samples were assessed according to Section 2.8.3.2. Then, the supernatant was collected, and its bile salt content was analyzed according to the method in Section 2.8.3.3.

2.8.3.6. Isothermal adsorption of bile salt by SDF. The optimum addition amount was determined according to the results obtained in Section 2.8.3.5. In accordance with the steps described in Section 2.8.3.2, different concentrations of bile salts (0.06, 0.12, 0.18, 0.24, or 0.3 mmol/L) were added to the digestive fluid samples, and the bile salt content was determined according to the method described in Section 2.8.3.3. The isotherms were plotted and fitted by empirical equation modeling. The adsorption isotherms were expressed in the form of the Freundlich equation (Eq. (4)).

$$\ln Qe = \frac{1}{n} \ln Ce + \ln K_f \quad (4)$$

where Qe is the equilibrium adsorption amount, mg/g; Ce is the equilibrium concentration, mg/g; n is a characteristic constant; and K_f is the equilibrium adsorption constant.

2.8.4. Determination of the inhibitory effect on pancreatic lipase

2.8.4.1. Determination of pancreatic lipase activity. The method of Yang et al. (Yang et al., 2010) was used with some modifications. Three 100 mL conical flasks were filled with 5 mL of 0.025 mol/L PBS (pH 7.4) and 4 mL of a 0.229 g/mL polyvinyl alcohol glycerol trioleate emulsion (substrate emulsion) and placed in an incubator for preheating at 37 °C for 10 min. Subsequently, 1 mL of 2 mg/mL tryptic lipase solution (prepared with pH 7.4 0.025 mol/L PBS buffer) was added, and the enzyme reaction was stopped immediately after 15 min of incubation by adding 15 mL of 95% ethanol. Then, three drops of phenolphthalein indicator were added, and a standard solution of 0.025 mol/L NaOH was slowly added until it the mixture was slightly red. A blank control was tested at the same time without the addition of pancreatic lipase solution. Fifteen milliliters of 95% ethanol was added immediately after 15 min of incubation, and finally, 1 mL of pancreatic lipase solution was added. Pancreatic lipase activity was calculated according to Eq. (5).

$$\text{Enzyme activity}(IU) = \frac{1000 \times (V_{sample} - V_{blank}) \times c}{t \times w} \quad (5)$$

where c is the concentration of the NaOH standard solution (mol/L); V_{sample} is the volume of NaOH standard solution consumed for the sample (mL); V_{blank} is the volume of NaOH standard solution consumed for the control (mL); t is the reaction time after enzyme addition (min); and w is the amount of pancreatic lipase added (g).

2.8.4.2. Determination of pancreatic lipase inhibition. PBS and the

substrate emulsion were added to a 100 mL triangular flask and incubated at 37 °C for 10 min. Then, a certain amount of SDF was added as a pancreatic lipase inhibitor, and the flask was kept warm for 10 min. Subsequently, 1 mL of pancreatic lipase solution was added, and the mixture was allowed to react for 15 min. Immediately after the end of the incubation, 15 mL of 95% ethanol was added to determine the residual enzyme activity. A blank was tested without the addition of SDF. One unit of inhibitor was considered to be inactivated by one unit of enzyme at pH 7.5 and a temperature of 37 °C. The rate of pancreatic lipase inhibition by SDF was calculated via Eq. (6).

$$\text{Inhibition ratio}(\%) = \frac{\text{Prior activity of pancreatic lipase} - \text{Later activity of pancreatic lipase}}{\text{Prior activity of pancreatic lipase}} \times 100 \quad (6)$$

2.8.4.3. Determination of the inhibition rate of pancreatic lipase by SDF. The inhibition rate was determined in accordance with the method described in Section 2.8.4.2 by varying the amount of SDF added (100 mg, 150 mg, 200 mg, 250 mg, or 300 mg). A regression curve was generated from the results with the amount of added SDF as the horizontal coordinate and the pancreatic lipase inhibition rate as the vertical coordinate to obtain the half maximal inhibitory concentration (IC_{50}) for pancreatic lipase inhibition.

2.8.4.4. Type of inhibition. Enzyme activity was determined according to the following 3 methods:

(a) Five milliliters of 0.025 mol/L PBS (pH = 7.4), 4 mL of substrate emulsion and 1 mL of pancreatic lipase solution were mixed and preheated for 15 min. Then, 150 mg of SDF was added, and the mixture was kept warm for 10 min. The reaction was stopped by the addition of 15 mL of 95% ethanol, after which the enzyme activity was measured.

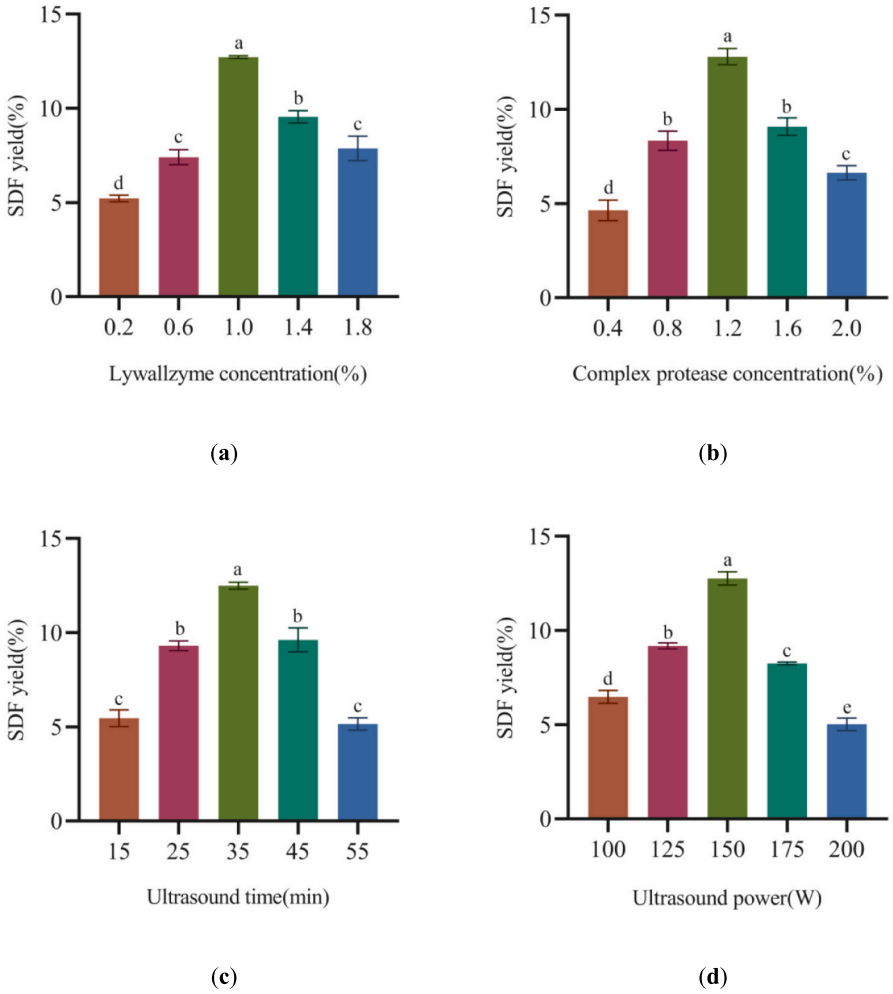

Fig. 2. Effects of independent variables on the SDF yield of *H. erinaceus*. The independent variables were tested with a Lywallzyme concentration of 1.0%, a complex protease concentration of 1.2%, an ultrasonication time of 35 min, and an ultrasonication power of 150 W as the default values while each independent variable was changed. (a) Lywallzyme concentration; (b) complex protease concentration; (c) ultrasonication time; (d) ultrasonication power. The data are shown as the mean ± standard deviation (n = 3). Bar charts with different letters are significantly different.

(b) First, 150 mg of SDF was preheated with 1 mL of pancreatic lipase solution for 15 min. Next, 5 mL of 0.025 mol/L PBS (pH = 7.4) and 4 mL of substrate emulsion were added, the mixture was incubated for 10 min, and then the reaction was stopped by the addition of 15 mL of 95% ethanol to determine the enzyme activity.

(c) First, 5 mL of 0.025 mol/L PBS buffer (pH = 7.4) was added, and then 4 mL of substrate emulsion was added to 150 mg of SDF and preheated for 10 min. Next, 1 mL of pancreatic lipase solution was added, the mixture was incubated for 15 min, and the reaction was stopped by the addition of 15 mL of 95% ethanol. The residual enzyme activity was determined, and the inhibition rate was calculated.

The type of inhibitory effect was determined as follows: 1 mL of 2 mg/mL pancreatic lipase solution was added to 2 or 4 mL of substrate emulsion to compare the responses with and without SDF addition at different substrate concentrations (sample group: 300 mg SDF addition; control group: 0 mg SDF addition). The Lineweaver–Burk double inverse method was used to plot 1/V against 1/[S] to analyze the effects of SDF addition on the type of inhibition of pancreatic lipase.

2.9. Statistical analysis

Each experiment was conducted in triplicate. Significant differences between groups were assessed by one-way analysis of variance (ANOVA) and Duncan's multiple comparison test using SPSS software (Statistical Products and Services Solutions, IBM SPSS Statistical Version 27, Armonk, New York, NY, USA). The standard deviation was used to express the data dispersion of the means. A p value <0.05 indicated a statistically significant difference. Origin 2021 and GraphPad Prism 8.0 software were used for plotting.

Table 2
Actual yield and predicted yield (in parentheses) of SDF from *H. erinaceus*.

Run	Coded Variable Levels				Yield of SDF (%)
	X_1	X_2	X_3	X_4	
1	1.0	2.0	55	150	5.89% (5.88%)
2	1.0	1.2	35	150	12.16% (12.69%)
3	1.8	1.2	15	150	6.67% (6.67%)
4	1.0	2.0	35	100	6.56% (6.55%)
5	1.0	2.0	15	150	6.05% (6.04%)
6	1.0	1.2	55	200	5.09% (5.08%)
7	1.0	1.2	35	150	12.65% (12.69%)
8	1.0	1.2	35	150	12.64% (12.69%)
9	0.2	1.2	35	100	5.85% (5.86%)
10	1.0	1.2	35	150	12.75% (12.69%)
11	1.0	2.0	35	200	5.83% (5.83%)
12	1.8	1.2	35	200	6.45% (6.44%)
13	1.0	1.2	15	100	5.97% (5.97%)
14	0.2	0.4	35	150	4.93% (4.92%)
15	1.0	0.4	35	200	4.83% (4.82%)
16	1.0	1.2	15	200	5.24% (5.22%)
17	1.8	1.2	55	150	6.51% (6.50%)
18	0.2	1.2	55	150	5.19% (5.17%)
19	1.8	2.0	35	150	7.25% (7.25%)
20	0.2	1.2	35	200	5.12% (5.12%)
21	1.0	1.2	35	150	12.65% (12.69%)
22	1.8	1.2	35	100	7.18% (7.18%)
23	0.2	1.2	15	150	5.34% (5.33%)
24	1.0	0.4	35	100	5.56% (5.57%)
25	1.0	0.4	55	150	4.90% (4.92%)
26	0.2	2.0	35	150	5.93% (5.90%)
27	1.8	0.4	35	150	6.26% (6.26%)
28	1.0	1.2	55	100	5.82% (5.81%)
29	1.0	0.4	15	150	5.05% (5.04%)

3. Results and discussion

3.1. Results of single-factor experiments

As shown in Fig. 2(a), the SDF extraction rate gradually increased at Lywallzyme concentrations between 0.2 and 1.0%. The extraction rate reached the maximum value at a Lywallzyme concentration of 1.0% and then showed a smooth decreasing trend. As shown in Fig. 2(b), the SDF extraction rate increased sharply at complex protease concentrations between 0.4% and 1.2% and then decreased. As shown in Fig. 2(c), the highest SDF extraction rate of 12.21% was achieved at an ultrasonication time of 35 min. The extraction rate decreased significantly at ultrasonication times exceeding 35 min. As shown in Fig. 2(d), the SDF extraction rate gradually increased as the ultrasonication power increased from 100 to 150 W and then decreased sharply with further increasing power.

3.2. RSM results

3.2.1. Model equation building and significance test

X_1 (Lywallzyme concentration), X_2 (complex protease concentration), X_3 (ultrasonication time), and X_4 (ultrasonication power) were used as variables, and the rate of SDF extraction from *H. erinaceus* was used as the response value. The average value from three parallel extractions was calculated, and the test conditions were in accordance with the design combinations provided by Design-Expert 10.0 software. The results are shown in Table 2.

Regression analysis of the experimental data was carried out using Design-Expert 10.0 software, and a regression equation was obtained for the percentage of SDF extracted from *H. erinaceus*. The corresponding regression equation is shown in Eq. (7).

$$\begin{aligned} Y = & 12.69 + 0.66X_1 + 0.50X_2 - 0.077X_3 - 0.36X_4 - 0.0025X_1X_2 \\ & - 0.0025X_1X_3 - 0.0025X_2X_4 - 3.07X_1^2 - 3.53X_2^2 - 3.69X_3^2 \\ & - 3.47X_4^2 \end{aligned} \quad (7)$$

where X_1, X_2, X_3 and X_4 represent the Lywallzyme concentration, complex protease concentration, ultrasonication time and ultrasonication power, respectively. The coefficient of determination was $R^2 = 0.9898$, which proved that the regression equation could be used to predict the theoretical SDF yield from *H. erinaceus*. The regression equation was subjected to ANOVA and significance testing, and the results are shown in Table 3. The F test showed that the model was significant with a high model F value (F = 14,553.24) and a low p value (p

Table 3
ANOVA results for the quadratic model of the extraction yield determined via RSM.

Source	Sum of Squares	DF	Mean Square	F Value	p Value
Model	207.38	14	14.81	14,553.24	<0.0001
X_1	5.28	1	5.28	5187.50	<0.0001
X_2	2.98	1	2.98	2927.75	<0.0001
X_3	0.071	1	0.071	69.30	<0.0001
X_4	1.60	1	1.60	1570.65	<0.0001
X_1X_2	2.500×10^{-5}	1	2.500×10^{-5}	0.15	0.7777
X_1X_3	2.500×10^{-5}	1	2.500×10^{-5}	0.15	0.7777
X_1X_4	0.000	1	0.000	0.000	1.0000
X_2X_3	2.500×10^{-5}	1	2.500×10^{-5}	0.15	0.7777
X_2X_4	0.000	1	0.000	0.000	1.0000
X_3X_4	0.000	1	0.000	0.000	1.0000
X_1^2	61.18	1	61.18	60,110.87	<0.0001
X_2^2	80.66	1	80.66	79,240.81	<0.0001
X_3^2	88.38	1	88.38	86,829.96	<0.0001
X_4^2	78.05	1	78.05	76,677.63	<0.0001
Residual	0.014	14	1.018×10^{-3}	–	–
Lack of Fit	5.000×10^{-5}	10	5.000×10^{-6}	1.408×10^{-3}	1.0000
Pure Error	0.014	4	3.550×10^{-3}	–	–
Cor Total	207.40	28	–	–	–

< 0.0001); therefore, the model could fully describe the relationships between the parameters. The linear regression coefficients X_1, X_2, X_3, and X_4 had low p values ($p < 0.0001$), indicating that the Lywallzyme concentration, complex protease concentration, ultrasonication time and ultrasonication power were significantly correlated with the SDF yield. A comparison of the F values of X_1, X_2, X_3 and X_4 indicated that the Lywallzyme concentration, complex protease concentration and ultrasonication power were the primary factors affecting the rate of SDF extraction, followed by the ultrasonication time.

3.2.2. Interactions between factors

To optimize the UAEE conditions, graphs were plotted to show the correlation between the response variable and the different levels of treatment variables, as well as the interactions between the variables. Fig. S1 shows a three-dimensional surface plot of the interactions between the factors. The other variables were at level 0, which corresponded to the optimal values obtained from the results of each single-factor experiment. Fig. S1(a) shows that the Lywallzyme concentration and complex protease concentration strongly affected the extraction rate of SDF from *H. erinaceus*. When the complex protease concentration was constant, the extraction rate first increased and then decreased with decreasing Lywallzyme concentration. Fig. S1(b) shows that the effect of the Lywallzyme concentration on the extraction rate of SDF was greater than that of the ultrasonication time. Fig. S1(d) shows that when the complex protease concentration was constant, the extraction rate first increased and then decreased with increasing ultrasonication time. According to Figs. S1(c), S1(e), and S1(f) and the F values in Table 3, the F values corresponding to X_1X_4, X_2X_4, and X_3X_4 were very low. Therefore, the linear and quadratic effects of all the independent variables on the studied response variable were significant ($p < 0.0001$). The interactions between the Lywallzyme concentration and ultrasonication power, between the complex protease concentration and ultrasonication power, and between the ultrasonication time and ultrasonication power were not significant.

3.2.3. Extraction process optimization and validation

The experimental results were analyzed via Design-Expert 10.0 software, and the optimal extraction conditions were a Lywallzyme concentration of 1.0%, complex protease concentration of 1.2%, ultrasonication time of 35 min, and ultrasonication power of 150 W; the predicted extraction rate was 12.69%. Three parallel experiments were carried out according to the above conditions, and the mean extraction rate was 12.48 ± 0.33%, which differed from the predicted extraction rate by 0.21%, indicating that the model can suitably predict the extraction rate of SDF from *H. erinaceus*.

In this study, two enzymes, Lywallzyme and complex protease, were used for the enzymatic extraction of SDF. Lywallzyme can hydrolyze the fungal cell wall and can increase the solubility of SDF inside the cell and on the cell wall, effectively increasing the yield of SDF. The complex protease enzymatically dissolved the proteins in the SDF solution, resulting in an increase in SDF purity. When the enzyme concentration was increased, the enzymatic reaction was more complete, and more SDF was solubilized. When the enzyme concentration was too high, the enzyme competed with the substrate, resulting in a certain amount of enzyme consumption, which led to a decrease in the SDF yield. In addition, the mechanical and cavitation effects of ultrasound can disrupt biological tissues such as cell walls and cell membranes and increase the mass transfer efficiency within the cell, thus promoting the release and extraction of SDF components (Wang, Cao, Wang, & Sun, 2011; Ponmurugan et al., 2017). However, when the ultrasonication time and ultrasonication power were too high, the structure of SDF fractured, and the SDF extraction rate gradually decreased. This was the reason why the yield of SDF decreased in the later stages of the single-factor experiments. The innovative combined use of Lywallzyme and ultrasonication to treat *H. erinaceus* solution described in this study effectively extracted SDF both inside and outside the cell and on the cell wall. Before the formal experiment began, a preexperiment was conducted. The final extraction rates of SDF were 2.41% and 5.62% with UAEE only and with Lywallzyme only, respectively. These results indicated that the combination of Lywallzyme and UAEE produced higher SDF yields. UAEE and Lywallzyme yielded better results and more convenient extraction parameters than did conventional hot water extraction. Wang et al. (Wang et al., 2015) compared ultrasound-assisted thermal extraction with conventional thermal extraction and reported that with ultrasound assistance, the yield increased by 16.34%, the temperature decreased by 13.3 °C, and the extraction time decreased by 37.78 min. Zhang et al. (Zhang, Jia, Liu, Wu, & Ran, 2011) extracted *Lycium barbarum* polysaccharides with UAEE in only 20 min, a much lower time than that required for enzymatic extraction (91 min).

Table 4
Basic components of SDF from *H. erinaceus* before and after purification.

	Moisture content	Protein	Starch	Ash content	SDF
Before purification	4.47 ± 0.05[a]	7.09 ± 0.14[a]	0.99 ± 0.04[a]	9.42 ± 0.52[a]	77.96 ± 0.44[a]
After purification	3.74 ± 0.25[a]	2.70 ± 0.17[b]	0.33 ± 0.07[b]	4.14 ± 0.26[b]	89.04 ± 0.65[b]

The data are shown as the mean ± standard deviation ($n = 3$). Different letters in the same column indicate significant differences ($p < 0.05$).

3.3. Basic composition and structural features of SDF

3.3.1. Basic composition

As shown in Table 4, purified SDF was obtained after deproteinization, depigmentation and purification by dialysis. Compared with that of the crude SDF, the purity of the purified SDF significantly increased ($p < 0.05$) by 11.08%, and the contents of protein, starch and ash significantly decreased ($p < 0.05$). The above results indicated that the SDF of *H. erinaceus* was sufficiently purified.

3.3.2. Molecular mass distribution of SDF

HPLC analysis of the SDF of *H. erinaceus* was carried out using coupled HPSEC-MALLS-RI. The corresponding chromatogram is shown in Fig. 3. There were three main peaks in the spectrum. The molecular mass of peak 1 was approximately 3.0×10^6 g/mol. The molecular mass of peak 2 was approximately 5.0×10^5 g/mol. The molecular mass of peak 3 was in the range of 4.0×10^4–9.0×10^4 g/mol. This further suggested that the molecular mass of the SDF from *H. erinaceus* was $>4.0 \times 10^4$ g/mol.

3.3.3. Monosaccharide composition of SDF

The monosaccharide composition of SDF is shown in Table 5 and Fig. 4. The SDF of *H. erinaceus* contained nine monosaccharides, including glucose, xylose, arabinose, fucose, mannose, rhamnose, galactose, galacturonic acid and glucuronic acid. Among them, galacturonic acid was the main monosaccharide in SDF, with a high content of 302.29 ± 6.53 μg/mg. Glucose, arabinose and galactose were present at relatively high levels, with contents of 38.78, 115.28, and 38.66 μg/mg, respectively. Among the identified monosaccharides, the most abundant were galacturonic acid, glucose, arabinose and galactose. Galacturonic acids are polymers linearly linked together by α-1,4 glycosidic bonds and are the major monosaccharides in pectin; the abundance of galacturonic acid observed in this study suggests that pectin may be an important component of SDF. Pectin is one of the major components of the cell wall, and Lywallzyme disrupts the structure of the cell wall, allowing pectin to be released. Pectin usually has a backbone that consists of galacturonic acid linked by α-D-1,4-glycosidic bonds and is attached to side chains by various glycosidic bonds (Chen et al., 2020). Xie et al. (Xie et al., 2022) investigated the physicochemical properties of SDF from grapefruit peel and showed that

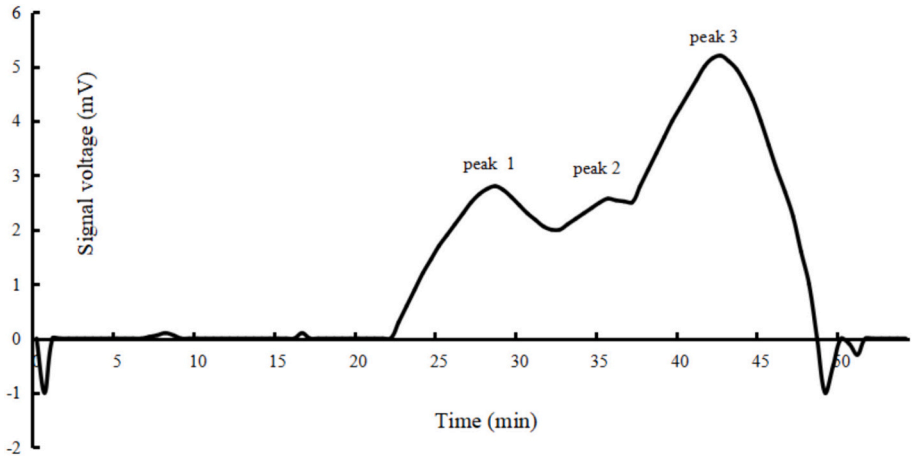

Fig. 3. High-performance liquid chromatography chromatograph indicating the molecular weight of *H. erinaceus* SDF.

Table 5
Composition and content of monosaccharides in *H. erinaceus* SDF.

Monosaccharide content (μg/mg)				
Glucose	Xylose	Galactose	Arabinose	Mannose
38.78 ± 1.65^{c}	6.21 ± 0.27^{e}	38.66 ± 1.34^{c}	115.28 ± 3.42^{b}	3.44 ± 0.14^{f}
Rhamnose	Fucose	Galacturonic acid	Glucuronic acid	
25.86 ± 1.03^{d}	1.98 ± 0.05^{g}	302.29 ± 6.53^{a}	1.57 ± 0.03^{h}	

The data are shown as the mean ± standard deviation ($n = 3$). Different letters in the same column indicate significant differences ($p < 0.05$).

galacturonic acid, arabinose and glucuronic acid were the main monosaccharide components; thus, pectin may be the main component. Yang et al. (Yang, Si, et al., 2022) investigated the physicochemical structure of SDF in coolgrass residue and reported that all SDF samples contained six monosaccharides: rhamnose, arabinose, galactose, glucose, xylose and galacturonic acid. These findings were consistent with the above experimental results.

3.4. Adsorption of oil by SDF

SDF reduces the amount of digested and absorbed fat in the gastrointestinal tract by binding to fat. The amount of soybean oil adsorbed by *H. erinaceus* SDF was 1.15 g/g. Thus, it was determined that *H. erinaceus* SDF has a certain adsorption capacity for fats. The oil binding capacity is one of the main parameters used to assess the ability of SDF to accelerate lipid excretion and lower serum cholesterol levels (Elleuch et al., 2010). SDF has a high oil binding capacity due to its porous surface structure. Sun et al. (Sun et al., 2024) investigated the bioactivity and adsorption properties of *Lentinus edodes* stalk DF and showed that *Lentinus edodes* stalk DF has a strong adsorption capacity for oils and fats. Qin et al. (Qin et al., 2023) extracted SDF from grapefruit peel to analyze its structural properties and adsorption capacity and observed good water and oil adsorption capacities. These findings are consistent with the results of this experimental study.

3.5. Adsorption of cholesterol micelles by SDF

The effect of the addition of different amounts of SDF on the adsorption of cholesterol micelles is shown in Fig. 5. The binding effect on cholesterol micelles increased with increasing *H. erinaceus* SDF content. The binding capacity reached a maximum when 150 mg of SDF was added. Under this condition, the binding capacity reached 11.91 mg/g.

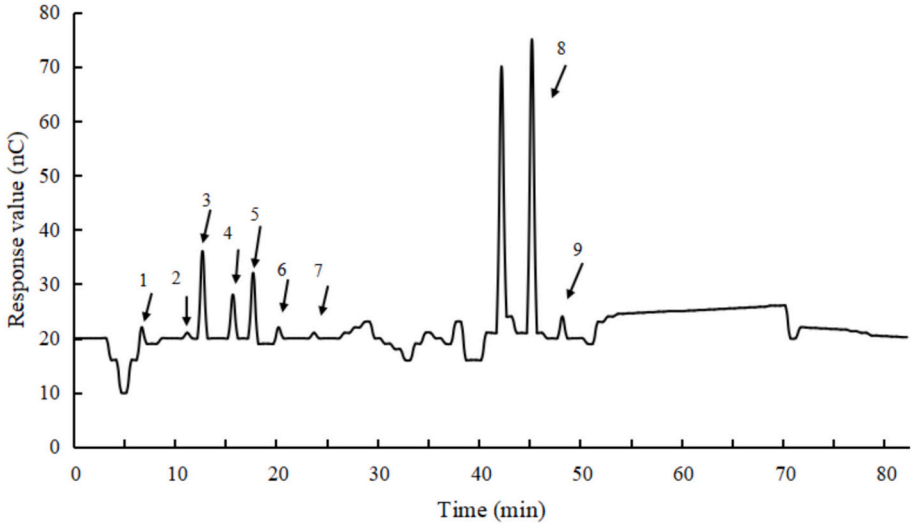

Fig. 4. High-performance anion exchange chromatograph of SDF monosaccharide composition. 1-Fucose; 2-rhamnose; 3-arabinose; 4-galactose; 5-glucose; 6-xylose; 7-mannose; 8-galacturonic acid; 9-glucuronic acid.

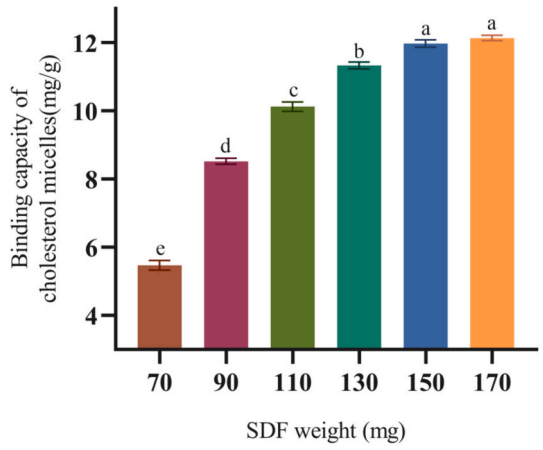

Fig. 5. Effect of SDF addition amount on the binding capacity of cholesterol micelles.

Afterward, the binding capacity with cholesterol micelles tended to stabilize. These findings indicate that *H. erinaceus* SDF has a certain hypolipidemic effect due to its ability to bind with cholesterol micelles to form precipitates.

3.6. Adsorption of bile salts by SDF

3.6.1. Full-wavelength scans of bile salts and corresponding standard curves

The sodium taurocholate solution and sodium glycocholate solution were subjected to full-wavelength scanning, as shown in Fig. S2. Both bile salt solutions exhibited a maximum absorption peak at 386 nm. The standard curves of the two bile salt solutions were obtained at a wavelength of 386 nm, as shown in Fig. S3. The correlation coefficient (R^2) values were 0.9989 and 0.9980 for sodium taurocholate and sodium glycocholate, respectively. Both standard curves showed good linearity.

3.6.2. Adsorption kinetics of bile salts by SDF

The amounts of bile salts adsorbed by SDF over time are shown in Fig. 6. The adsorption of bile salts by SDF first increased rapidly with time and then began to stabilize after 60 min. When the reaction time reached 90 min, the adsorption of bile salts reached saturation. The binding amount and binding rate of sodium taurocholate were greater than those of sodium glycocholate. At 90 min, the binding amount and binding rate of sodium taurocholate were 3.73 mg/g and 42.47%, respectively, and those of sodium glycocholate were 3.43 mg/g and 39.12%. In subsequent experiments, we chose 90 min as the optimal reaction time.

3.6.3. Effect of SDF addition on the amount of bound bile salts

Fig. 7 shows the effect of the addition of different SDF concentrations on the amount of bound bile salts. With increasing amounts of SDF, the amount of bound bile salts tended to first increase and then decrease. When the amount of SDF reached 190 mg, the SDF adsorption capacities for bile salts reached the highest values of 3.97 mg/g and 3.86 mg/g for sodium taurocholate and sodium glycocholate, respectively. For subsequent experiments, we chose 190 mg as the optimal amount of SDF added.

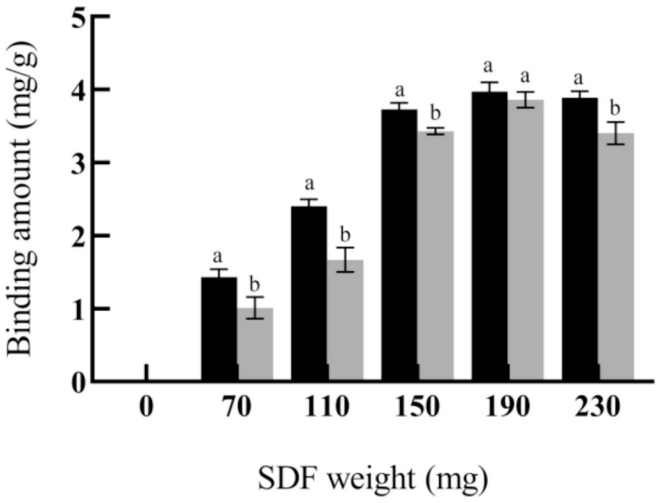

Fig. 7. Effect of SDF addition on the amount of bound bile salts. Black represents sodium taurocholate, and gray represents sodium glycylcholate. For identical SDF weights, different letters represent significant differences.

Table 6
Fitting parameters of the adsorption isotherms.

Bile salts	Freundlich equation	N	In K_f	R^2
Sodium taurocholate	In Qe = 1.0666In Ce+2.6057	0.9376	2.6057	0.9989
Sodium glycocholate	In Qe = 1.3623In Ce+2.9401	0.7341	2.9401	0.9940

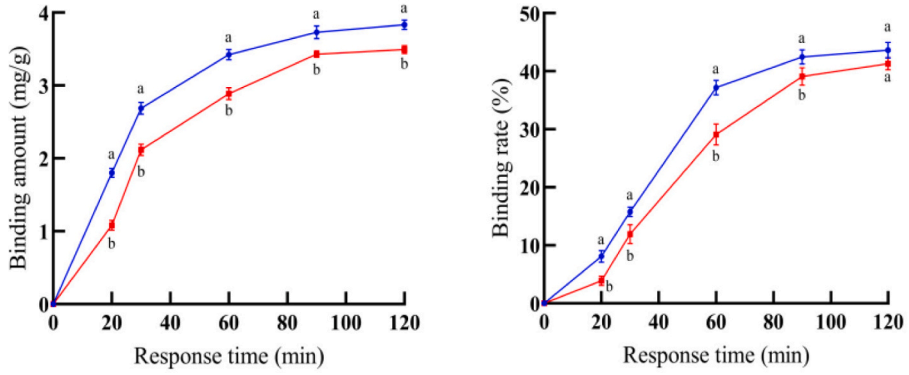

(a) **(b)**

Fig. 6. Adsorption kinetics of bile salts by SDF. The blue curve represents sodium taurocholate, and the red curve represents sodium glycocholate. (a) Binding amount; (b) binding rate. For identical response times, different letters represent significant differences. (For interpretation of the references to color in this figure legend, the reader is referred to the web version of this article.)

3.6.4. Isothermal adsorption of bile salts by SDF

As shown in Fig. S4, the binding rates gradually increased and then decreased with increasing bile salt concentration, and the binding amounts also increased. The binding amount of sodium taurocholate was always greater than that of sodium glycocholate. This result was consistent with the above findings.

The adsorption isotherms were fitted by the Freundlich equation, and the results are shown in Fig. S5 and Table 6. The fitted equations were obtained on the basis of the fitted curves. In this case, the R^2 values were 0.9989 and 0.9940 for sodium taurocholate and sodium glycocholate, respectively, which showed that the fitted curves had a good linear relationship. This result was consistent with the Freundlich isothermal adsorption equation, in which the N value indicates the strength of the effect of the addition amount on the adsorption capacity. According to the Freundlich model, adsorption can easily occur when 1/n is between 0.1 and 0.5 and cannot easily occur if the 1/n value is >2.0 (Amrutha, Gautham, Chikmagalur, & Balakrishna, 2023). The experimental results showed that SDF had some adsorption capacity for bile salts, but the adsorption capacity was weak.

The bile salt adsorption capacity is an important index for evaluating the lipid-lowering properties of SDF (Lu, Hua, Yuge, Lei, Jie, Sierkemideke, et al., 2015). Research has shown that some naturally obtained polysaccharides can combine with bile salts to stimulate the rapid decomposition of cholesterol in the liver into bile acids; these bile acids combine with Na^+ and K^+ and participate in human liver and intestinal circulation, where they regulate cholesterol metabolism and accelerate the digestion and absorption of fats, thus lowering blood lipids (Li et al., 2024). SDF has a high water swelling capacity, can increase the viscosity of the medium, and can interact to form a network structure, which contributes to the adsorption of bile acid salt (Gil-López et al., 2019; Ma & Mu, 2016). Sodium taurocholate and sodium glycocholate are the main bile salts present in the digestive system (F, H. A., 2009). This study demonstrated the capacity of *H. erinaceus* SDF to adsorb both sodium taurocholate and sodium glycocholate. Gao et al. (Gao, Lin, Sun, & Zhao, 2017) investigated the hypolipidemic function of kelp polysaccharides and found that kelp polysaccharides have a significant bile salt binding capacity, which may be related to their specific structural features. Wang et al. (Wang et al., 2018) studied the adsorption capacity of rice bran polysaccharides for bile salts and showed that the binding capacities for sodium taurocholate and sodium deoxycholate were 24.96 and 13.63 μmol/100 mg, respectively. These findings are in accordance with the above experimental results.

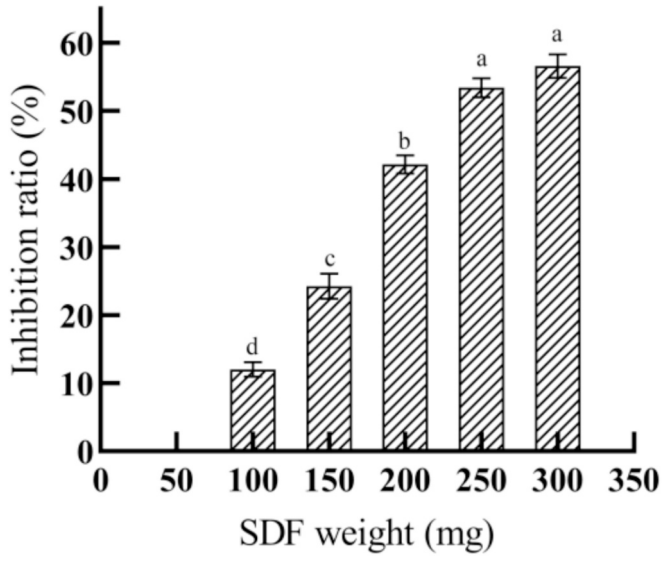

Fig. 8. SDF inhibition rate of pancreatic lipase at different concentrations. Bar charts with different letters are significantly different.

3.7. Inhibition of pancreatic lipase by SDF

3.7.1. Determination of the inhibition rate of pancreatic lipase under SDF addition

Fig. 8 shows the effect of SDF addition on the inhibition of pancreatic lipase. As shown in the figure, *H. erinaceus* SDF, an inhibitor, tended to inhibit pancreatic lipase activity to a greater degree as the amount of SDF increased, but the increase plateaued.

The equation for the inhibitory effect of SDF on pancreatic lipase activity was obtained by generating a regression curve with the logarithm of added SDF as the horizontal coordinate and the inhibition rate as the vertical coordinate, as shown in Fig. S6. In this case, R^2 was 0.9987, and IC_{50} was 223.67 mg.

3.7.2. Type of inhibition

The substrate emulsion, the inhibitor and pancreatic lipase were added in different orders, and the observed pancreatic lipase inhibition differed for different orders of addition. The experimental results (Fig. S7) showed that addition of the materials in order 3 yielded the highest inhibition rate. Therefore, SDF reacted with the substrate first and hindered the interaction of the substrate emulsion with pancreatic lipase, thus inhibiting pancreatic lipase activity. Fig. 9 shows a Lineweaver–Burk plot of pancreatic lipase inhibition by SDF. The two straight lines for the added inhibitor group and the no inhibitor group intersect the vertical axis. Pancreatic lipase inhibition by *H. erinaceus* SDF was competitive in nature. Competitive inhibition indicates that when the structures of the inhibitor and the substrate are similar, they will compete for the same binding site on the enzyme, preventing the substrate from binding to the enzyme and leading to a decrease in the rate of the enzyme-catalyzed reaction (Zhou, Li, Wu, Fan, & Ouyang, 2015).

This study showed that *H. erinaceus* SDF has an inhibitory effect on pancreatic lipase activity. The reason for the decrease in pancreatic lipase activity may be that the combination of pancreatic lipase with the functional groups of SDF changed the three-dimensional structure of the enzyme, which resulted in decreased pancreatic lipase activity (Qi et al., 2015). The inhibition of pancreatic lipase activity by SDF was competitive. When 300 mg of SDF was added and the substrate concentration was low, the substrate did not decompose. As the substrate concentration increased, the mixed solution became acidic, indicating that at this point, the substrate was being broken down by pancreatic lipase. This may be because at lower substrate concentrations, SDF competed with tryptic lipase for binding sites and bound to the substrate first, preventing tryptic lipase from breaking down the substrate. When the substrate concentration increased, the inhibitor bound to only a portion of the substrate, so pancreatic lipase could break down the remaining substrate. Regarding the inhibition of pancreatic lipase activity by the inhibitor, it has also been found that with increasing inhibitor addition, the internal hydrophobic region of the active site of pancreatic lipase becomes increasingly exposed (Raj, 2008). Serine residues containing hydroxyl groups are acylated, leading to irreversible inactivation of the enzyme. The inactivated enzyme is unable to hydrolyze fats into fatty acids and monoglycerides, so undigested triglycerides are excreted in the feces (Cao, Mei, Mehmood, Sun, & Chen, 2024; D'Costa, Emily, Radia, Kaden, & Nicolas, 2024). Studies have shown that polysaccharides can inhibit the absorption of fat in the small intestine by inhibiting pancreatic lipase activity (Takahiro et al., 2007). Yu et al. (Yu et al., 2023) found that citrus peel DF inhibited pancreatic lipase activity. DF can change the secondary structure of pancreatic lipase by decreasing the content of α-helical structures and increasing the content of β-folded structures, which may lead to opening of its structure and exposure of its active site. The mechanism underlying the inhibition of pancreatic lipase by this inhibitor needs to be studied more thoroughly.

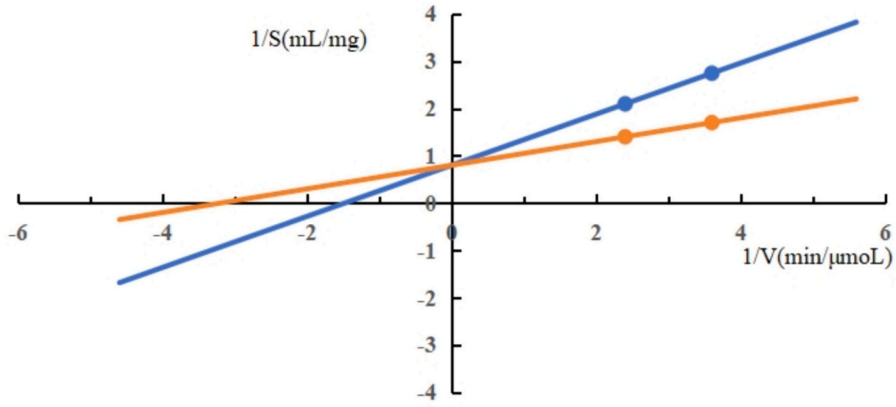

Fig. 9. Lineweaver–Burk plot. The blue curve represents the inhibitor group, and the orange curve represents the no inhibitor group. (For interpretation of the references to color in this figure legend, the reader is referred to the web version of this article.)

4. Conclusion

In this study, SDF was extracted from the fruiting bodies of *H. erinaceus*. On the basis of the results of single-factor experiments, the UAEE extraction process was optimized via Design-Expert software, a mathematical model was established, and the following optimal extraction conditions were obtained: Lywallzyme concentration, 1.0%; complex protease concentration, 1.2%; ultrasonication time, 35 min; and ultrasonication power, 150 W. The optimal conditions were reasonable and reliable, and the corresponding yield of *H. erinaceus* SDF was 12.48%. *H. erinaceus* SDF had a strong ability to adsorb oil, cholesterol micelles, sodium taurocholate and sodium glycocholate. In addition, SDF had a certain inhibitory effect on pancreatic lipase activity. Lipid-lowering effects could be achieved by adsorbing bile salts to accelerate cholesterol decomposition and conversion and inhibit pancreatic lipase activity. This study provides a reference for the development of lipid-lowering and lipid-related functional mushroom foods. In this study, only in vitro lipid-lowering effects were investigated, and the specific mechanism involved needs to be investigated and verified via in vivo experiments. Therefore, further studies are needed in the future.

Funding

This work was supported financially by Shanghai Agricultural Commission Program (2020-02-08-00-12-F01479) and Shanghai Academy of Agricultural Sciences (JCYJ231601).

CRediT authorship contribution statement

Panling Yu: Writing – original draft, Validation, Methodology, Investigation, Formal analysis, Data curation, Conceptualization. **Xueyu Pan:** Writing – review & editing. **Mingjie Chen:** Resources, Funding acquisition. **Jianshuai Ma:** Software, Investigation, Data curation. **Baoting Xu:** Validation, Formal analysis. **Yan Zhao:** Writing – review & editing, Supervision, Resources, Project administration, Conceptualization.

Declaration of competing interest

The authors declare no conflicts of interest.

The authors declare that they have no known competing financial interests or personal relationships that could have appeared to influence the work reported in this paper.

Data availability

The data presented in this study are available in the article.

Acknowledgments

The authors acknowledge the resources and laboratory facilities provided by the Institute of Edible Fungi, Shanghai Academy of Agricultural Sciences.

Appendix A. Supplementary data

Supplementary data to this article can be found online at https://doi.org/10.1016/j.fochx.2024.101657.

References

Amrutha, A., Gautham, J., Chikmagalur, R. G., & Balakrishna, P. (2023). Development of a multicomponent adsorption isotherm equation and its validation by modeling. *J. Langmuir: the ACS journal of surfaces and colloids, 39*, 17862–17878.

Bistriche, G. E., Hoffmann, S. F. A., & Wenzel, d. M. E.. (2022). The effects of soluble dietary fibers on glycemic response: An overview and futures perspectives. *J. Foods., 11*(23), 3934.

Cai, W., Ding, Z., Wang, Y., Yang, Y., Zhang, H., & Yan, J. (2019). Hypoglycemic benefit and potential mechanism of a polysaccharide from Hericium erinaceus in streptozotoxin-induced diabetic rats. *J. Process Biochemistry, 88*(C), 180–188.

Cao, Q., Mei, S., Mehmood, A., Sun, Y., & Chen, X. (2024). Inhibition of pancreatic lipase by coffee leaves-derived polyphenols: A mechanistic study. *J. Food chemistry., 444*, 138514.

Cassidy, Y. M., McSorley, E. M., & Allsopp, P. J. (2018). Effect of soluble dietary fibre on postprandial blood glucose response and its potential as a functional food ingredient. *J. Journal of Functional Foods., 46*, 423–439.

Chen, F., Geng, W., Li, X., Chen, L., Xu, C., Huang, W., & Ming, Y. (2023). Optimization of the ultrasonic-assisted enzymatic extraction of polysaccharides from;Dendrobium offcinale;Kimura et Migo and bioactivity study. *J. CyTA - Journal of Food., 21*(1), 692–700.

Chen, T., Zhang, Z., Wang, Z., Chen, Z., Ma, H., & Yan, J. (2020). Effects of ultrasound modification at different frequency modes on physicochemical, structural, functional, and biological properties of citrus pectin. *J. Food Hydrocolloids, 106484*.

D'Costa, A. S., D'Costa, A. S., Emily, H., Radia, E., Kaden, V., & Nicolas, B. (2024). Impact of potato starch on the inhibition of pancreatic lipase by potato phenolic acids. *J. Food Bioscience., 57*, 103414.

Duan, D., Ma, F., Zhao, L., Ying, Y., Zheng, Y., Xu, X., Sun, Y., & Xue, Y. (2022). Variation law and prediction model to determine the moisture content in tea during hot air drying. *J. Journal of Food Process Engineering., 45*(2).

Elleuch, M., Bedigian, D., Roiseux, O., Besbes, S., Blecker, C., & Attia, H. (2010). Dietary fibre and fibre-rich by-products of food processing: Characterisation, technological functionality and commercial applications: A review. *J. Food Chemistry., 124*(2), 411–421.

F, H. A.. (2009). Bile acids: Trying to understand their chemistry and biology with the hope of helping patients. *J. Hepatology (Baltimore, Md.), 49*(5), 1403–1418.

Bakr, A. F., & Farag, M. A. (2023). Soluble dietary fibers as Antihyperlipidemic agents: A comprehensive review to maximize their health benefits. *J. ACS omega., 8*(28), 24680–24694.

Gao, J., Lin, L., Sun, B., & Zhao, M. (2017). Comparison study on polysaccharide fractions from Laminaria japonica: Structural characterization and bile acid binding capacity. *J. Journal of agricultural and food chemistry., 65*(44), 9790–9798.

Gerarda, G. A., Raffaele, P., Salvatore, A., Giovanna, P., Giovanni, B., Rossella, D. O., … Alessandro, F. (2023). Hericium erinaceus, a medicinal fungus with a centuries-old history: Evidence in gastrointestinal diseases. *J. World journal of gastroenterology., 29*(20), 3048–3065.

Gil-López, D. I. L., Lois-Correa, J. A., Sánchez-Pardo, M. E., Domínguez-Crespo, M. A., Torres-Huerta, A. M., Rodríguez-Salazar, A. E., & Orta-Guzmán, V. N. (2019). Production of dietary fibers from sugarcane bagasse and sugarcane tops using microwave-assisted alkaline treatments. *J. Industrial Crops & Products., 135*, 159–169.

Guan, Z., Yu, E., & Feng, Q. (2021). Soluble dietary Fiber, one of the Most important nutrients for the gut microbiota. *J. Molecules., 26*(22), 6802.

Guo, Q., Liang, S., Xiao, Z., & Ge, C. (2023). Research progress on extraction technology and biological activity of polysaccharides from edible Fungi: A review. *J. Food Reviews International., 39*(8), 4909–4940.

Hua, M., Liu, Z., Sha, J., Li, S., Dong, L., & Sun, Y. (2021). Effects of ginseng soluble dietary fiber on serum antioxidant status, immune factor levels and cecal health in healthy rats. *J. Food Chemistry., 365*, 130641.

Ji, H., Yu, J., Dong, X., & Liu, A. (2019). Preparation of soluble dietary fibers from Gracilaria lemaneiformis and its antitumor activity in vivo. *J. Journal of Food Measurement and Characterization., 13*(2), 1574–1582.

Jia, F., Liu, X., Gong, Z., Cui, W., Wang, Y., & Wang, W. (2020). Extraction, modification, and property characterization of dietary fiber from Agrocybe cylindracea. *J. Food science & nutrition., 8*(11).

Li, B., Chen, X., Wu, H., Su, J., Ding, Y., Zhang, Z., Rong, M., Dong, Y., He, X., Li, L., Lv, G., & Chen, S. (2024). The anti-hyperlipidemia effect of Atractylodes macrocephala rhizome increased HDL via reverse cholesterol transfer. *J. Heliyon., 10*(7), Article e28019.

Li, D., Chen, M., Meng, X., Sun, Y., Liu, R., & Sun, T. (2024). Extraction, purification, structural characteristics, bioactivity and potential applications of polysaccharides from Avena sativa L.: A review. *J. International journal of biological macromolecules, 265*(P2), 130891.

Li, Q., Dou, Z., Duan, Q., Chen, C., Liu, R., Jiang, Y., Yang, B., & Fu, X. (2024). A comparison study on structure-function relationship of polysaccharides obtained from sea buckthorn berries using different methods: Antioxidant and bile acid-binding capacity. *J. Food Science and Human Wellness., 13*(01), 494–505.

Lily, S. I. A. H., Afaf, K., Usama, S. S. A. D. A., Leila, C. I., & Serene, H. (2023). Soluble and insoluble dietary fibre in date fruit varieties: An evaluation of methods and their implications for human health. *J. Foods., 12*(6), 1231.

Liu, J., Guo, Y., Sun, J., Lei, Y., Guo, M., & Wang, L. (2024). Extraction methods, multiple biological activities, and related mechanisms of Momordica charantia polysaccharide: A review. *J. International Journal of Biological Macromolecules, 263*(P2), 130473.

Liu, J., Wang, W., Hu, Q., Wu, X., Xu, H., Su, A., Xie, M., & Yang, W. (2022). Bioactivities and molecular mechanisms of polysaccharides from Hericium erinaceus. *J. Journal of Future Foods., 2*(2), 103–111.

Liu, Y., Zhao, Y., Yang, Y., Tang, Q., Zhou, S., Wu, D., & Zhang, J. (2013). Structural characteristics and hypoglycemic activity of polysaccharides from Coprinus comatus. *J. Bioactive Carbohydrates and Dietary Fibre., 2*(2), 164–169.

Ma, M., & Mu, T. (2016). Effects of extraction methods and particle size distribution on the structural, physicochemical, and functional properties of dietary fiber from deoiled cumin. *J. Food Chemistry., 194*, 237–246.

Minato, K., Laan, L., Die, I., & Mizuno, M. (2019). Pleurotus citrinopileatus polysaccharide stimulates anti-inflammatory properties during monocyte-to-macrophage differentiation. *J. International Journal of Biological Macromolecules, 122*.

Moczkowska, M., Karp, S., Niu, Y., & Kurek, M. (2019). Enzymatic, enzymatic-ultrasonic and alkaline extraction of soluble dietary fibre from flaxseed – A physicochemical approach. *J. Food Hydrocolloids., 90*, 105–112.

Perry, J. R., & Wu, Y. (2016). A review of physiological effects of soluble and insoluble dietary fibers. *J. Nutrition & Food Sciences., 6*(2), 1–6.

Ponmurugan, K., Al-Dhabi, N., Maran, J., Karthikeyan, K., Moothy, I., Sivarajasekar, N., & Manoj, J. (2017). Ultrasound assisted pectic polysaccharide extraction and its characterization from waste heads of Helianthus annus. *J. Carbohydrate Polymers, 173*.

Qi, J., Li, Y., Yokoyama, W., Majeed, H., Masamba, K., Zhong, F., & Ma, J. (2015). Cellulosic fraction of rice bran fibre alters the conformation and inhibits the activity of porcine pancreatic lipase. *J. Journal of Functional Foods., 19*, 39–48.

Qin, X., Dong, X., Tang, J., Chen, Y., Xie, J., Chen, Y., Zheng, B., Hu, X., & Yu, Q. (2023). Comparative analysis of dietary fibers from grapefruit peel prepared by ultrafine grinding: Structural properties, adsorption capacities, in vitro prebiotic activities. *J. Food Bioscience., 56*.

Raederstorff, D., Schlachter, M., Elste, V., & Weber, P. (2003). Effect of EGCG on lipid absorption and plasma lipid levels in rats. *J. The Journal of Nutritional Biochemistry., 14*(6), 326–332.

Raj, P. (2008). Cetilistat, a new lipase inhibitor for the treatment of obesity. *J. Current opinion in investigational drugs (London, England : 2000)., 9*(4), 414–421.

Shang, H., Song, H., Shen, S., Yao, X., Wu, B., Wang, L., Jiang, Y., & Ding, G. (2015). Effects of dietary polysaccharides from the submerged fermentation concentrate of Hericium caput-medusae (bull.:Fr.) Pers. on fat deposition in broilers. *J. Journal of the science of food and agriculture., 95*(2), 267–274.

Shao, L., Sun, Y., Liang, J., Li, M., & Li, X. (2020). Decolorization affects the structural characteristics and antioxidant activity of polysaccharides from Thesium chinense Turcz: Comparison of activated carbon and hydrogen peroxide decolorization. *J. International Journal of Biological Macromolecules., 155*, 1084–1091.

Shehzad, H., Minaxi, S., & Rajeev, B. (2021). Valorisation of sea buckthorn pomace by optimization of ultrasonic-assisted extraction of soluble dietary fibre using response surface methodology. *J. Foods., 10*(6), 1330.

Sheng, Y., Zhao, C., Zheng, S., Mei, X., Huang, K., Wang, G., & He, X. (2019). Anti-obesity and hypolipidemic effect of water extract from Pleurotus citrinopileatus in C57BL/6J mice. *J. Food science & nutrition., 7*(4).

Sun, L., Wen, L., Li, Q., Chen, R., Wen, S., Lai, X., Lai, Z., Cao, J., Zhang, Z., Hao, M., Cao, F., & Sun, S. (2024). Microbial fermentation enhances the effect of black tea on hyperlipidemia by mediating bile acid metabolism and remodeling intestinal microbes. *J. Nutrients., 16*(7).

Sun, Y., Li, B., Xue, Y., Wang, J., Miao, B., Liu, Y., Li, Y., Cao, Y., & Chang, D. (2024). Comparison of immunomodulatory activity of polysaccharides and soluble dietary fibers and adsorption capacities of insoluble dietary fibers extracted from Lentinus edodes stipes. *J. Food Production, Processing and Nutrition., 6*(1).

Takahiro, T., Hiroe, T., Takeshi, T., Toshiya, S., Naoyuki, Y., & Jun, H. (2007). Inhibition of lipase activities by basic polysaccharide. *J. Journal of lipid research., 48*(2), 358–365.

Tanaka, Y., Okamoto, K., Matsushima, A., Ota, T., Matsumoto, Y., & Akasaki, T. (2013). Microwave-assisted acid hydrolysis of Konjac products for determining the Konjac powder content;original papers. *J. Analytical Sciences., 29*(11), 1049–1053.

Thanchanit, T., & Pornanong, A. (2017). A review of the efficacy, safety, and clinical implications of naturally derived dietary supplements for dyslipidemia. *J. American journal of cardiovascular drugs : drugs, devices, and other interventions., 17*(1), 27–35.

Tu, J., Liu, H., Wen, Y., Chen, P., & Liu, Z. (2021). A novel polysaccharide from Hericium erinaceus: Preparation, structural characteristics, thermal stabilities, and antioxidant activities in vitro. *J. Journal of food biochemistry., 45*(9), e13871.

Wang, J., Cao, Y., Wang, C., & Sun, B. (2011). Low-frequency and low-intensity ultrasound accelerates alliinase-catalysed synthesis of allicin in freshly crushed garlic. *J. Journal of the science of food and agriculture., 91*(10).

Wang, Q., Niu, L., Liu, H., Wu, Y., Li, M., & Jia, Q. (2021). Structural characterization of a novel polysaccharide from Pleurotus citrinopileatus and its antitumor activity on H22 tumor-bearing mice. *J. International Journal of Biological Macromolecules, 168*.

Wang, W., Li, J., Lu, F., & Liu, F. (2024). Ultrasound-assisted multi-enzyme extraction for highly efficient extraction of polysaccharides fromUlva lactuca. *J. Foods., 13*(6).

Wang, W., Ma, X., Xu, Y., Cao, Y., Jiang, Z., Ding, T., Ye, X., & Liu, D. (2015). Ultrasound-assisted heating extraction of pectin from grapefruit peel: Optimization and comparison with the conventional method. *J. Food Chemistry, 178*.

Wang, Y., Yu, G., Zang, X., & Ye, F. (2018). Optimization, antioxidant activity and bile salts adsorption capacity of the aqueous enzymatic extract from rice bran. *J. Czech Journal of Food Sciences., 36*, 338–348.

Wen, L., Zhang, Z., Zhao, M., Senthamaraikannan, R., Padamati, R., Sun, D., & Tiwari, B. (2020). Green extraction of soluble dietary fibre from coffee silverskin: Impact of ultrasound/microwave-assisted extraction. *J. International Journal of Food Science & Technology, 55*(5), 2242–2250.

Xie, J., Peng, G., Hu, X., Xie, J., Chen, Y., Dong, R., Si, J., Yang, C., & Yu, Q. (2022). Physicochemical characteristics of soluble dietary Fiber obtained from grapefruit Peel insoluble dietary Fiber and its effects on blueberry jam. *J. Foods., 11*(22), 3735.

Yan, J., Hu, J., Yang, R., & Zhao, W. (2018). A new nanofibrillated and hydrophobic grafted dietary fibre derived from bamboo leaves: Enhanced physicochemical properties and real adsorption capacity of oil. *J. International Journal of Food Science & Technology, 53*(10), 2394–2404.

Yang, C., Si, J., Chen, Y., Xie, J., Tian, S., Cheng, Y., Hu, X., & Yu, Q. (2022). Physicochemical structure and functional properties of soluble dietary fibers obtained by different modification methods from Mesona chinensis Benth. Residue. *J. Food Research International., 157*, 111489.

Yang, J., Ma, X., Zhang, Z., Chen, B., Li, S., & Wang, G. (2010). Lipase immobilized by modification-coupled and adsorption–cross-linking methods: A comparative study. *J. Biotechnology Advances., 28*(5), 644–650.

Yu, B., Tang, Q., Fu, C., Regenstein, J., Huang, J., & Wang, L. (2023). Effects of different particle-sized insoluble dietary fibre from citrus peel on adsorption and activity inhibition of pancreatic lipase. *J. Food Chemistry., 398*, 133834.

Yuan, L., Qiu, Z., Yang, Y., Liu, C., & Zhang, R. (2022). Preparation, structural characterization and antioxidant activity of water-soluble polysaccharides and purified fractions from blackened jujube by an activity-oriented approach. *J. Food chemistry., 385*, 132637.

Zhang, J., Jia, S., Liu, Y., Wu, S., & Ran, J. (2011). Optimization of enzyme-assisted extraction of the Lycium barbarum polysaccharides using response surface methodology. *J. Carbohydrate Polymers., 86*(2).

Zhang, M., Yao, M., Jia, A., Shi, Y., Bai, X., Liu, X., Cui, T., Liu, X., & Liu, C. (2021). Hypolipidemic effect of soluble dietary fibers prepared from Asparagus officinalis and their effects on the modulation of intestinal microbiota. *J. Food Science and Biotechnology., 30*(13), 1721–1731.

Zhang, N., Huang, C., & Ou, S. (2011). In vitro binding capacities of three dietary fibers and their mixture for four toxic elements, cholesterol, and bile acid. *J. Journal of Hazardous Materials., 186*(1), 236–239.

Zhang, Z., Yu, A., Hu, W., Wu, L., Yang, D., Fu, L., Wang, Z., Kuang, H., & Wang, M. (2024). A review on extraction, purification, structural characteristics, biological activities, applications of polysaccharides from Hovenia dulcis Thunb. (Guai Zao). *J. International journal of biological macromolecules, 265*(P2), 131097.

Zhou, D., Li, L., Wu, Y., Fan, J., & Ouyang, J. (2015). Salicylic acid inhibits enzymatic browning of fresh-cut Chinese chestnut (Castanea mollissima) by competitively inhibiting polyphenol oxidase. *J. Food Chemistry., 171*, 19–25.

Zhou, K., Xia, W., Zhang, C., & Yu, L. (2005). In vitro binding of bile acids and triglycerides by selected chitosan preparations and their physico-chemical properties. *J. LWT - Food Science and Technology., 39*(10), 1087–1092.

Zhuang, H., Dong, H., Zhang, X., & Feng, T. (2023). Antioxidant activities and prebiotic activities of water-soluble, alkali-soluble polysaccharides extracted from the fruiting bodies of the fungus Hericium erinaceus. *J. Polymers., 15*(20).